Cerebral Cortex, December 2021;31: 5497–5510

https://doi.org/10.1093/cercor/bhab174
Advance Access Publication Date: 28 June 2021
Original Article

ORIGINAL ARTICLE

A Cortical Surface-Based Meta-Analysis of Human Reasoning

Minho Shin[1] and Hyeon-Ae Jeon[1,2]

[1]Department of Brain and Cognitive Sciences, Daegu Gyeongbuk Institute of Science and Technology (DGIST), Daegu 42988, Korea and [2]Partner Group of the Max Planck Institute for Human Cognitive and Brain Sciences at the Department of Brain and Cognitive Sciences, DGIST, Daegu 42988, Korea

Address correspondence to Hyeon-Ae Jeon. Email: jeonha@dgist.ac.kr

Abstract

Recent advances in neuroimaging have augmented numerous findings in the human reasoning process but have yielded varying results. One possibility for this inconsistency is that reasoning is such an intricate cognitive process, involving attention, memory, executive functions, symbolic processing, and fluid intelligence, whereby various brain regions are inevitably implicated in orchestrating the process. Therefore, researchers have used meta-analyses for a better understanding of neural mechanisms of reasoning. However, previous meta-analysis techniques include weaknesses such as an inadequate representation of the cortical surface's highly folded geometry. Accordingly, we developed a new meta-analysis method called Bayesian meta-analysis of the cortical surface (BMACS). BMACS offers a fast, accurate, and accessible inference of the spatial patterns of cognitive processes from peak brain activations across studies by applying spatial point processes to the cortical surface. Using BMACS, we found that the common pattern of activations from inductive and deductive reasoning was colocalized with the multiple-demand system, indicating that reasoning is a high-level convergence of complex cognitive processes. We hope surface-based meta-analysis will be facilitated by BMACS, bringing more profound knowledge of various cognitive processes.

Key words: Bayesian meta-analysis of the cortical surface (BMACS), functional magnetic resonance imaging, inductive and deductive reasoning, integrated nested Laplace approximation (INLA), log-Gaussian Cox process

Introduction

Reasoning is one of the uniquely human cognitive processes (Penn et al. 2008; Heit and Rotello 2010). Among different categories of reasoning, inductive reasoning involves inferring underlying relations from several instances (Wertheim and Ragni 2018). Existing knowledge is intricated with inductive reasoning for making predictions about novel objects or contexts (McAbee et al. 2017), and thus, various cognitive processes are involved in inductive reasoning such as categorization, probability judgment, analogical thinking, inference, and decision-making (Klauer and Phye 2008; Hayes et al. 2014). With respect to deductive reasoning, this process requires inferring a definitive conclusion from given information (Goel 2005). People work with a set of premises and derive a conclusion that is not explicitly stated on the initial premises, and thus, several mental processes are engaged for successful performance in deduction such as premise encoding, premise integration, and conclusion validation (Rodriguez-Moreno and Hirsch 2009). Both inductive reasoning and deductive reasoning hinge on multiple mental processes which dynamically interact with each other, being intrinsic to human high-level cognition (Heit and Rotello 2010).

The fact that reasoning is central to human cognitive processes has attracted many researchers to interrogate its underlying neural mechanisms. With respect to inductive reasoning, several regions such as the left inferior frontal gyrus, precentral gyrus and superior frontal gyrus, bilateral middle frontal gyrus, bilateral superior parietal lobule, right precuneus, left inferior parietal lobule, and right superior occipital gyrus were reported to be actively involved (Wertheim and Ragni 2018). In analogy—a type of inductive reasoning—researchers claimed that the left frontopolar cortex is necessary for the processing of induction (Green et al. 2010). In terms of deductive reasoning, a "core" region of deductive reasoning was found in the left rostrolateral prefrontal cortex and medial superior frontal gyrus (Monti et al. 2009). Meta-analyses have been conducted in this regard, showing that the right middle frontal gyrus, left medial frontal gyrus, and bilateral posterior parietal cortex were actively involved in deductive reasoning (Prado et al. 2011). Another study observed bilateral occipital, parietal, temporal, and frontal lobes; basal ganglia; and cerebellar regions as a large brain network for deductive reasoning (Goel 2007). As described here, a large and varied set of regions in the human brain has been reported for these 2 reasoning processes, with some of the regions being overlapped or differentiated. Thus, there has not been a clear answer to the question of whether or not a central neural process exists in different types of reasoning. Findings in most of the previous neuroimaging studies have focused on either inductive-specific or deductive-specific reasoning, and it is hard to find studies where the 2 processes were compared directly with each other within a single study. Therefore, in the present study, we investigated the core neural underpinnings of reasoning by combining inductive and deductive reasoning together, hoping to find the differences as well as commonalities of neural mechanisms across the 2 types of reasoning.

In spite of the recent advances in neuroimaging techniques, there has been controversy over the low statistical power of individual neuroimaging studies (Button et al. 2013), primarily resulting from small sample sizes (typically 20–30 participants per study). A recent study showed that results were highly variable even from a single dataset when analyzed by different research groups (Botvinik-Nezer et al. 2020). One way of overcoming these problems and producing coherent results from a large number of individual studies is to conduct a meta-analysis. The meta-analysis of neuroimaging studies has been performed mostly using *x*, *y*, and *z* coordinates of brain activations, known as a coordinate-based meta-analysis, as neuroimaging studies usually report peak locations of brain activations (i.e., peak *x*, *y*, and *z* coordinates) rather than whole-brain statistical maps. The 2 well-known methods for coordinate-based meta-analysis are a multilevel kernel density analysis (MKDA) (Wager et al. 2007) and an activation likelihood estimation (ALE) (Turkeltaub et al. 2002). These methods construct study-specific maps by convolving kernels (e.g., a 10 mm sphere) with foci (i.e., a set of reported peak coordinates) from individual studies. The study-specific maps are then collapsed into a single image, being thresholded by significance testing. A series of these processes reveal significant brain voxels that are consistently activated across studies. MKDA and ALE are often called "kernel-based methods," since the analyses entail convolving foci with some types of kernels.

Even though kernel-based methods have been widely used in neuroimaging communities, there are a small number of concerns. Firstly, kernel-based meta-analyses are based on a mass-univariate approach consisting of a number of univariate statistical tests, testing each voxel independently. As a consequence, these methods often ignore the nature of spatial dependence of neuroimaging data such as long-range correlations as well as local correlations of activity among brain areas (Bowman 2005). Secondly, the spatial kernel parameters (e.g., the radius of spheres in MKDA and standard deviation of Gaussian kernels in ALE) are determined arbitrarily, being independent of how the foci are distributed in the brain. There are no rigorous guidelines on choosing spatial kernel parameters satisfactorily such that the parameters are determined empirically or based on sample size (Eickhoff et al. 2009), let alone reflecting how the foci are distributed. Moreover, this arbitrarily selected kernel is applied to the whole brain regardless of foci locations, which is biologically implausible because the degree of spatial dependence would vary across brain regions (Penny et al. 2005). Most importantly, the spatial kernels do not properly represent the highly folded geometry of the cortical surface because the underlying assumption behind the setup of kernels implies that the neural activation would propagate over the volumetric space. As a result, the distance between 2 points on the neighboring gyri is regarded as much closer than the actual distance on the cortical surface when the distance is considered in volumetric space (Dale et al. 1999).

As an alternative to the kernel-based methods, model-based methods grounded on spatial statistics theories such as Bayesian meta-analytic methods have been suggested to resolve the concerns regarding the conventional meta-analysis mentioned above (Kang et al. 2011, 2014; Yue et al. 2012; Montagna et al. 2018; Samartsidis et al. 2019). The Bayesian model-based methods, which estimate the posterior distribution of the spatial model parameters, enable us to obtain various information from the model, such as activation strength of a particular location in the brain or the effect of a covariate (e.g., age) on a specific cognitive process. Furthermore, these methods allow us to build predictive maps for different cognitive processes, which are known to outperform the results from a naive classifier based on kernel-based methods (Samartsidis et al. 2017).

However, the Bayesian model-based methods also have weaknesses. They are complicated to use and require considerable computing resources and processing time, which may hinder practitioners from conducting Bayesian meta-analysis easily. In addition, to the best of our knowledge, no Bayesian methods have introduced cortical surface-based analysis to date. Thus, they still convey one of the major problems of kernel-based approaches, that is, ignorance of the highly folded geometry of cortical surface. To overcome these shortcomings, we need a new way of meta-analysis that is not only reliable and precise but also easily accessible and fast in computation that accurately models the spatial dependence of the data.

Putting the 2 issues (i.e., the neural underpinnings of reasoning and the issue of meta-analysis) together, researchers have strived to unveil the core brain regions involved in the reasoning process through coordinate-based meta-analyses. However, as mentioned earlier, the conventional kernel-based approaches used in previous analyses still have some weaknesses. Moreover, the question of which brain regions are crucial to the reasoning process has not been properly addressed, since previous studies focused on studying different kinds of reasoning separately instead of adopting a comprehensive approach that includes different reasoning processes together. Therefore, we suggest 2 solutions to overcome these problems. One is to develop a fast, accurate, and reliable meta-analysis method, and the other is to take a comprehensive approach to the understanding of general mechanisms related to inductive and deductive

reasoning by using a substantial number of studies. To this end, we developed a new meta-analysis method, called Bayesian meta-analysis of the cortical surface (BMACS), in which we adopted log Gaussian Cox processes (LGCPs) (Møller et al. 1998; Samartsidis et al. 2019) to define explicit spatial modeling and confined the regions of interest to the cortical surface to better reflect the complexly folded cortical layer structure (Mejia et al. 2020). LGCPs are a class of models that are known to infer true spatial patterns even from incompletely observed patterns such as a set of points, which are flexible but easily tractable (Diggle et al. 2013). Furthermore, for parameter estimation, BMACS used integrated nested Laplace approximation (INLA; Rue et al. 2009) that is known to require less computation and to provide more accurate estimation in most circumstances (Rue et al. 2017) compared to a common method called Markov chain Monte Carlo (MCMC; Gamerman and Lopes 2006) that is known to provide a precise estimation but needs substantial computation. As a result, BMACS offers a fast, accurate, and reliable model-based meta-analysis.

An overview of our new meta-analysis, BMACS, is displayed in Figure 1. We initially collected foci from 76 studies that examined either inductive or deductive reasoning. After additional screening to perform meta-analysis of the cortical surface, the coordinates from 74 studies in the volumetric coordinate system were accurately mapped to the surface coordinate system (Wu et al. 2018). One might raise an issue of inaccurate mapping between the 2 coordinate systems. However, we would argue that we took the most appropriate and rigorous approach, considering only a scarce number of publicly shared individual studies using cortical surface-based analysis in the current neuroimaging community. After transferring all the foci to the spherical surface, we applied the LGCP (Møller et al. 1998) to estimate spatial maps for each reasoning process. Then, we mapped core regions related to inductive and deductive reasoning using exceedance probability such that we could rigorously scrutinize different as well as common activated patterns of each reasoning process. BMACS was further validated in multiple steps with different analyses to confirm its reliability.

Materials and Methods

Data Collection

We collected our data following Preferred Reporting Items for Systematic Reviews and Meta-Analyses (Moher et al. 2009). The procedure is explained in detail as follows.

1. Identification: We collected 986 studies from the PubMed database. The exact search keyword was "(Reasoning [Title/Abstract] OR 'Transitive Inference' [Title/Abstract]) AND (fMRI OR functional magnetic resonance imaging OR PET OR Positron Emission Tomography)," and we limited the publication date till 31 December 2019. Additionally, we included 102 studies that had been included in previous meta-analyses (Prado et al. 2011; Wendelken 2015; Hobeika et al. 2016; Wertheim and Ragni 2018). After removing duplicated studies, we collected 996 studies in total.
2. Screening: We first screened irrelevant studies based on their titles. Therefore, studies other than human neuroimaging with healthy adults were excluded (e.g., clinical reasoning or topics unrelated to human reasoning), resulting in 208 remaining studies.
3. Eligibility: We further excluded studies that did not contain whole-brain analysis (e.g., region of interest [ROI] analysis or conjunction analysis only). Also, studies with incomplete description of functional data were removed (e.g., omission in scanning parameters such as a voxel size or a slice gap). Lastly, we excluded one study where all the x, y, z coordinates were reported as positive values, regardless of their locations. Finally, 76 studies were included for the current study.
4. Included: 76 studies were filtered with respect to reasoning in functional magnetic resonance imaging (fMRI) or positron emission tomography studies. Subsequently, we only included contrast maps if they were classified into one of the following categories: 1) simple task contrasts, 2) contrasts compared to baseline conditions, 3) contrasts compared to the other reasoning tasks, 4) contrasts that compared different conditions within reasoning, 5) contrasts with parametric effects, and 6) contrasts that looked for interaction effects. These categories were applied to both inductive and deductive reasoning. As a result, we obtained 2207 foci within 265 contrasts in the 76 studies. The detailed information about the included studies and contrast maps were released in http://doi.org/10.5281/zenodo.4638499.

Preprocessing

According to the advice on neuroimaging meta-analysis (Müller et al. 2018), we located all the foci from different brain templates into the Montreal Neurological Institute (MNI) space with MATLAB R2020a (MathWorks Inc., MA), using the following 4 strategies:

1. If the functional data were normalized with the statistical parametric mapping (SPM) standard template but the peak coordinates were reported in Talairach coordinates without mentioning any transformations from MNI coordinates to Talairach ones, they were categorized as MNI coordinates.
2. If the peak coordinates were transformed from MNI coordinates to Talairach coordinates using Brett transformation (Brett et al. 2001), we used *tal2mni* function (Brett et al. 2001) to *unbrett* the coordinates. The functions related to Brett transformation were obtained from https://imaging.mrc-cbu.cam.ac.uk/imaging/MniTalairach.
3. If transforming MNI coordinates using Lancaster transformation (Lancaster et al. 2007) were mentioned in a paper, we applied *tal2icbm* function (Lancaster et al. 2007). The functions related to Lancaster transformation were obtained from https://brainmap.org/icbm2tal/.
4. If the functional data were normalized into Talairach space and the peak coordinates were reported in Talairach coordinates, we applied Lancaster transformation (*tal2icbm*) (Lancaster et al. 2007).

For cortical surface-based analysis, we additionally transformed the MNI coordinates onto the fsaverage surface (Fischl et al. 1999) using RF-ANTs (v0.11.1), which is a nonlinear mapping method that has been known to enable accurate mapping between the 2 coordinate systems (Wu et al. 2018). Specifically, we mapped the coordinates onto the sphere-shaped fsaverage surface. A sphere-shaped surface has an advantage over surfaces of other shapes, because the estimation process of random field is easier on a sphere. We could not complete the mapping of 585 coordinates (out of 2207 coordinates) onto the cortical surface through the conversion process, because they were reported outside of the MNI brain or the gray matter in the cortex. Among the remaining 1622 coordinates, we additionally removed coordinates from 2 deductive reasoning studies, which reported a large number of foci (i.e., 170 136 foci) that could potentially bias the results. As a result, our dataset contains

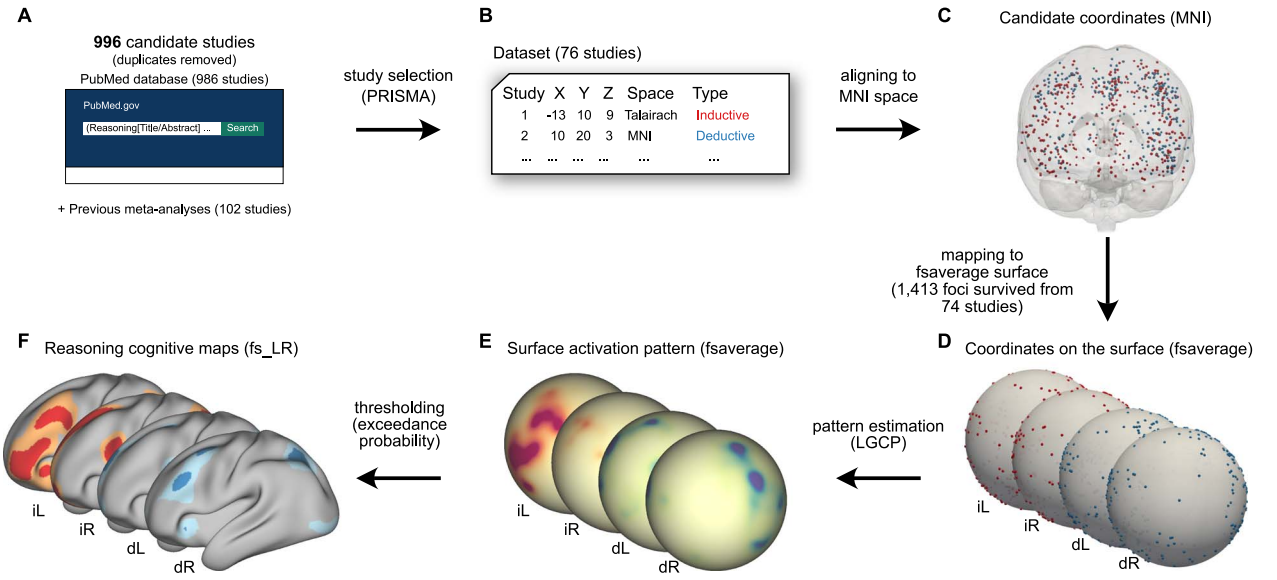

Figure 1. Overview of BMACS. (*A*) Searching the PubMed database and incorporating additional studies from previous meta-analyses, we first included 996 candidate studies for our meta-analysis of reasoning. (*B*) After following the suggestions by Preferred Reporting Items for Systematic Reviews and Meta-Analyses (PRISMA; Moher et al. 2009), 76 studies were filtered for the meta-analysis. (*C*) The acquired foci were then located in the standard MNI coordinate system. (*D*) Subsequently, the foci were mapped onto the fsaverage surface for each reasoning process and hemisphere, respectively, resulting in the final dataset of 1413 foci from 74 studies (iL, inductive Left; iR, inductive Right; dL, deductive Left; dR, deductive Right). (*E*) Using LGCPs, BMACS estimated reasoning-specific maps such as inductive reasoning (orange-red) and deductive reasoning (teal-cyan). (*F*) Finally, the results were mapped onto the fs_LR surface (Van Essen et al. 2012) and thresholded using exceedance probability for visualization. Darker colors correspond to regions with above 95% exceedance probability (highly related regions), and lighter colors correspond to regions with above 50% exceedance probability (moderately related regions).

1413 coordinates from 227 contrasts in 74 studies. Among the 74 studies, 4 studies reported contrasts related to both inductive and deductive reasoning. Here, we separated such studies into 2 independent studies, one being an inductive-specific study and the other being a deductive-specific study to model study-specific effects. We will therefore indicate the number of studies as 78 in the remaining of the paper although the actual included number of studies is 74. In total, each inference included 39 studies, respectively. The preprocessed data are available from http://doi.org/10.5281/zenodo.4638499.

Bayesian Meta-Analysis of the Cortical Surface

In the present study, we introduced BMACS. BMACS assumes that the point patterns are generated by LGCPs (Møller et al. 1998) on the cortical surface. Here, the unit of observation was an individual study, which means we considered each set of foci reported from individual studies as separate point patterns generated by the latent spatial point processes. Given the intensity surface $\lambda(s)$ and a point set Y, the likelihood of a LGCP (Simpson et al. 2016) is defined as

$$\pi(Y|\lambda) = \exp\left\{|\Omega| - \int_{\Omega} \lambda(s)ds\right\} \prod_{y \in Y} \lambda(y), \quad (1)$$

where the intensity λ is given as

$$\lambda(s) = \exp\{Z(s)\} \quad (2)$$

at a location $s \in \Omega$ with $Z(s)$ being a Gaussian random field. In BMACS, Ω is a unit sphere, representing the cortical hemisphere unfolded into a sphere, and $|\Omega|$ is the area of a unit sphere (i.e., $4\pi^2$). Point set Y is a set of coordinates reported in previous reasoning fMRI studies. Finally, the intensity λ represents the activation strength over the cortical surface. The likelihood to observe a point set Y given an intensity λ increases when Y contains points with high intensities (i.e., highly observable regions). In addition, the integral of intensity $\lambda(s)$over the surface Ω (i.e., $\int_{\Omega}\lambda(s)ds$) is the expected number of points to be observed over the surface Ω.

The latent field $Z(s)$ is then modeled as

$$Z(s) = \mu + x(s), \quad (3)$$

where μ is a constant mean over the space and x is a spatially varying random field that is constructed by a Matérn covariance structure, which is more flexible at explaining the spatial variance than the common squared exponential covariance function (Lindgren and Rue 2015).

Since each hemisphere is mapped onto the separate cortical surface, we considered foci from different hemispheres as foci from separate spheres. Also, we modeled a common random effect α_i for each study i. By introducing a random effect for each study, BMACS relaxes the assumption of independence within points from the same studies and prevents the possibility of biased estimates driven by only a few studies (Samartsidis et al. 2019). Subsequently, by extending equation (2) to incorporate random effects for studies, intensity λ for each study i and hemisphere h is given as

$$\lambda_{i,h}(s) = \alpha_i \exp\{\mu_{r_i,h} + x_{r_i,h}(s)\}, \quad (4)$$

where $i = 1, 2, \ldots, 78, r_i \in \{\text{inductive, deductive}\}, h \in \{\text{left, right}\}$.

The major computational bottleneck of previous Bayesian meta-analysis methods was the process of MCMC (Gamerman

and Lopes 2006) for posterior estimation. To speed up the computation of posterior estimates, we applied an approximate inference method called INLA, which is implemented in the R-INLA package v21.02.23 (Rue et al. 2009). Additionally, to make inference of the random field more feasible, we adopted a stochastic partial differential equation (SPDE), and thus, we approximated a continuous Matérn spatial field, which produces fast as well as stable inference (Lindgren et al. 2011; Simpson et al. 2012). We used 6252 vertices to approximate the spatially varying random field x for computational feasibility (Mejia et al. 2020). For priors, default priors of R-INLA were used for parameters in BMACS, unless mentioned otherwise. Briefly, for SPDE specification, priors for 2 parameters of the Matérn field were $\log(\tau) \sim \mathcal{N}(-3.22, 10)$ and $\log(\kappa) \sim \mathcal{N}(1.95, 10)$, where the means of the prior distributions were decided depending on the spatial resolution of the surface. The default prior for the random effects of studies was $\log(\alpha_i) \sim \mathcal{N}(0, 1/p)$, where the log precision p was set as $\log p \sim \mathcal{G}(1, 0.00005)$. All the relevant codes for BMACS and further analysis are available from http://doi.org/10.5281/zenodo.4638499.

Posterior Analysis

One thousand posterior samples of the maps for each reasoning r and hemisphere h were obtained after regressing out the random effects from each study as

$$\lambda_{r,h}^{k}(s) = \exp\left\{\mu_{r,h}^{k} + x_{r,h}^{k}(s)\right\}, \tag{5}$$

where $r \in \{\text{inductive, deductive}\}$, $h \in \{\text{left hemisphere, right hemisphere}\}$, and $k = 1, 2, \ldots, 1000$ representing 1000 posterior draws.

Exceedance probability refers to the probability that a parameter would be greater than or less than a value, being computed from posterior distribution of the parameter (Bolin and Lindgren 2015). Using this exceedance probability, we found regions that are most likely to be engaged in the reasoning processes. Specifically, we searched for regions where the probabilities that intensity λ would exceed one are greater than a threshold p. Intensity λ for a Poisson distribution is interpreted as that λ events are expected to occur within the unit interval. In other words, when λ is greater than one, we expect more than one event to occur during the reasoning process in survived regions. The exceedance probability is formulated as

$$\Pr\left(\lambda(s) \geq 1\right) = \frac{1}{K}\sum_{k=1}^{K} \mathrm{II}\left(\lambda^{k}(s) \geq 1\right), \tag{6}$$

where K is the number of posterior draws and $\mathrm{II}(\cdot)$ refers to an indicator function that is 1 if pointwise intensity $\lambda(s)$ is equal to or greater than 1, or 0 otherwise. To further describe the results into the multimodal parcellation of the Human Connectome Project, the exceedance probability maps were mapped onto the fs_LR surface (Van Essen et al. 2012). We set the threshold of the exceedance probability P as 0.95 and considered the regions that survived the threshold as highly related regions. The reported regions of interests were described according to the multimodal parcellation of the Human Connectome Project (Glasser, Coalson, et al. 2016a).

Bayesian Spatial Point Process Classifier

Inferring the cognitive states from the observed neural activity is known as reverse inference or, in general, brain decoding (Poldrack 2006; Yarkoni et al. 2011). In line with this, one important question to be addressed in the present study was whether or not the estimated mental representations (i.e., spatial activation patterns) would accurately identify inductive-specific or deductive-specific processes. To determine if this was possible, based on a previous study (Kang et al. 2014), we built a classifier using the inductive- and deductive-specific activation maps estimated by BMACS and scrutinized its ability to correctly decode the type of reasoning of a newly presented brain activation map. We used leave-one-study-out cross-validation (LOOCV) as a measure to evaluate the performance of BMACS. Usually, we need to re-run BMACS N times to compute LOOCV accuracy, in which N is the number of studies included. Even though it takes significantly less time to run BMACS compared to previous Bayesian meta-analysis methods, it is still inefficient to fit the model repetitively since the number of studies included in a meta-analysis typically exceeds 20, and in the current study, 78. In other words, we would have to have fitted the model 78 times for the present study. Therefore, for more efficient computation, we approximated LOOCV using importance sampling without multiple refittings (Gelfand et al. 1992; Gelfand 1996; Kang et al. 2014). The LOOCV probability that the label T_i of a new pointset Y_i is classified as j given observed data $\mathcal{D}_{-i}$ is approximated using posterior draws of the parameters that were estimated from the full data $\mathcal{D}$ (Kang et al. 2014) as

$$\hat{\Pr}\left[T_i = j | Y_i, \mathcal{D}_{-i}\right] = \frac{p_j \hat{Q}_{jt_i}}{\sum_{j'=1}^{J} p_{j'} \hat{Q}_{j't_i}}. \tag{7}$$

Because the denominator of equation (7) is just a normalizing term, we only computed the numerator, where p_j is prior probability that a new point set would be classified as label j (either inductive or deductive reasoning), and $\hat{Q}_{jt_i}$ is

$$\hat{Q}_{jt_i} = \frac{1}{K}\sum_{k=1}^{K} \frac{\pi\left(Y_i | \lambda_j^k\right)}{\pi\left(Y_i | \lambda_{t_i}^k\right)}, \tag{8}$$

where t_i is the true label of study i and K is the number of simulations from approximated posterior distribution, which is 1000 posterior draws in the current study.

Here, $\pi(Y_i | \lambda_j^k)$ is

$$\pi\left(Y_i | \lambda_j^k\right) = \pi\left(Y_i | \lambda_{j,\text{left}}^k\right) + \pi\left(Y_i | \lambda_{j,\text{right}}^k\right). \tag{9}$$

The predicted label $\hat{T}_i$ of a new pointset Y_i is then given by

$$\hat{T}_i = \arg\max_j \left(p_j \hat{Q}_{jt_i}\right). \tag{10}$$

Multilevel Kernel Density Analysis

We additionally performed another meta-analysis using MKDA (Wager et al. 2007; Wager et al. 2009) (available from https://github.com/canlab/Canlab_MKDA_MetaAnalysis) to scrutinize

whether the results from BMACS were comparable to those from a conventional meta-analysis (i.e., MKDA).

We used 1413 foci that survived conversion to fsaverage space, such that BMACS and MKDA had the same number of foci for the analysis. The peak coordinates were convolved with a spherical kernel of 10 mm in radius, then a binary indicator map was produced with the value of one in the location of convolved peaks or else zero for each of the 78 studies, which were aggregated with convolved peaks in a study. After calculating a weighted average of the indicator maps, 5000 Monte Carlo simulations were performed to set a threshold for a null hypothesis that peaks would be uniformly distributed throughout the gray matter. Voxels were considered to be significant at $P < 0.05$, family-wise error rate corrected for multiple comparison. We rendered the MKDA results onto the cortical surface to directly compare the results of MKDA depicted in the volumetric space with the results of BMACS depicted on the cortical surface (Marcus et al. 2011).

We also built reverse inference maps from MKDA and performed a LOOCV using a Naive Bayes Classifier (NBC) (Yarkoni et al. 2011). The classification accuracy from NBC was later used as a baseline to compare how BMACS performs in terms of classification.

Validation of BMACS on a Working Memory Dataset

BMACS adopts several strategies to analyze the data on the cortical surface instead of the volumetric space and to approximate the posterior distributions of the model parameters using INLA (Rue et al. 2009). To validate whether BMACS is able to draw compatible results with other Bayesian methods, we applied BMACS to the publicly available working memory dataset (Rottschy et al. 2012) that had previously been analyzed using another Bayesian meta-analytic method (Samartsidis et al. 2019) called a Bayesian random-effects meta-regression model, which used MCMC on the volumetric space. We elucidated how the results from the 2 methods (BMACS and the Bayesian random-effects meta-regression model) were comparable to each other. We tried to reproduce 3 core results: 1) the comparison of probabilities of observing at least one peak coordinate for ROIs between verbal and nonverbal working memory, 2) the effects of age and sample size on working memory, and 3) variability in random effects between studies.

The model specification for each study j defined in the original study (Samartsidis et al. 2019) is as follows:

$$\lambda_{j,h}(s) = \alpha_j \exp\left\{\mu_{v_j,h} + \beta_1 \text{age}_j + \beta_2 \frac{1}{\sqrt{n_j}} + x_{v_j,h}(s)\right\}, \qquad (11)$$

where $v_j \in \{\text{verbal, nonverbal}\}$, and $h \in \{\text{left hemisphere, right hemisphere}\}$. Covariates age_j and n_j refer to mean age and the total sample size of study j, respectively.

Probability of Observing At least One Focus in ROIs

The probability of observing at least one peak coordinate in an ROI B is expressed as $\Pr\{N(B) \geq 1\}$, where $N(\cdot)$ refers to the number of observed foci in an ROI. It can be formulated into the probability that more than one event would occur in a ROI using Poisson distribution with intensity Λ_B as $1 - Pois(x = 0; \Lambda_B)$, where $\Lambda_B = \int_B \lambda(s)ds$. Since the authors in the original paper (Samartsidis et al. 2019) used the Harvard-Oxford Atlas to define ROIs, we applied the same atlas, mapping it onto the cortical surface and computing the probability for each ROI.

Effects of Age and Sample Size on Working Memory

We tried to reproduce the effects of covariates, namely age and sample size, of the original paper (Samartsidis et al. 2019). From the estimated model using BMACS, we derived the marginal posterior distribution of coefficients of age and sample size. The effects of covariates were considered to be significant if the 95% highest density interval of the covariates did not contain zero.

Variability of random effects

In the original paper (Samartsidis et al. 2019), the authors assumed the prior distribution of random effects to be a Gamma distribution as $\alpha_i \sim \mathcal{G}(10, 10)$ to let 90% of the density be within [0.5,1.5]. Likewise, we embedded similar prior information for the random effects α_i by setting the prior distribution of random effects to be the log-normal distribution with mean as 0, variance as 0.1, such that $\log(\alpha_i) \sim \mathcal{N}(0, 0.1)$.

Simulation

To further validate our model, we performed a simulation study and examined whether our model recovers true parameters well. We set the true parameters as posterior means of the estimates from BMACS and generated one point set for each formulated study using equation (4), resulting in 78 simulated point sets. The parameters were considered to be successfully recovered if the 95% highest density intervals derived from the marginal posterior distribution of parameters contained the true parameters.

Results

Reasoning-Specific Maps Revealed by BMACS

Using BMACS, we found regions that were specifically activated in inductive and deductive reasoning as well as the commonly activated regions (Fig. 2; see Supplementary Fig. S1 for unthresholded maps). Here, the abbreviations for the brain regions were borrowed from the multimodal parcellation of the Human Connectome Project (Glasser, Coalson, et al. 2016a). Only the regions that are easily shown in Figure 2 are stated here (for the full list of anatomical labeling of the activated parcels and their abbreviations, see Supplementary Table S1).

We revealed areas commonly activated in both types of reasoning processes (Fig. 2A): the dorsolateral prefrontal cortex (8C, p9-46v), inferior frontal cortex (p47r, IFSp), orbital and polar frontal cortex (a47r), anterior cingulate and medial prefrontal cortex (8BM), insular and frontal opercular cortex (AVI), and paracentral lobular and mid cingulate cortex (SCEF) in the left hemisphere. Activations in the right hemisphere were smaller than those in the left hemisphere, being located in the dorsolateral prefrontal cortex (p9-46v), inferior/superior parietal cortex (IP1, MIP, LIPd), anterior cingulate and medial prefrontal cortex (8BM), and paracentral lobular and mid-cingulate cortex (SCEF).

In inductive reasoning (Fig. 2B), several activations were observed in the left hemisphere in addition to the common regions: the inferior frontal cortex (IFJp, and IFSa), inferior parietal cortex (IP1), premotor cortex (6r), and visual cortex (V1). Much smaller extent of activations was observed on the right hemisphere than the left hemisphere: insular and frontal opercular cortex (AVI), premotor cortex (6r), and early visual cortex (V3).

In deductive reasoning (Fig. 2C), in addition to the common regions, a broad expanse of the left frontal lobe was observed

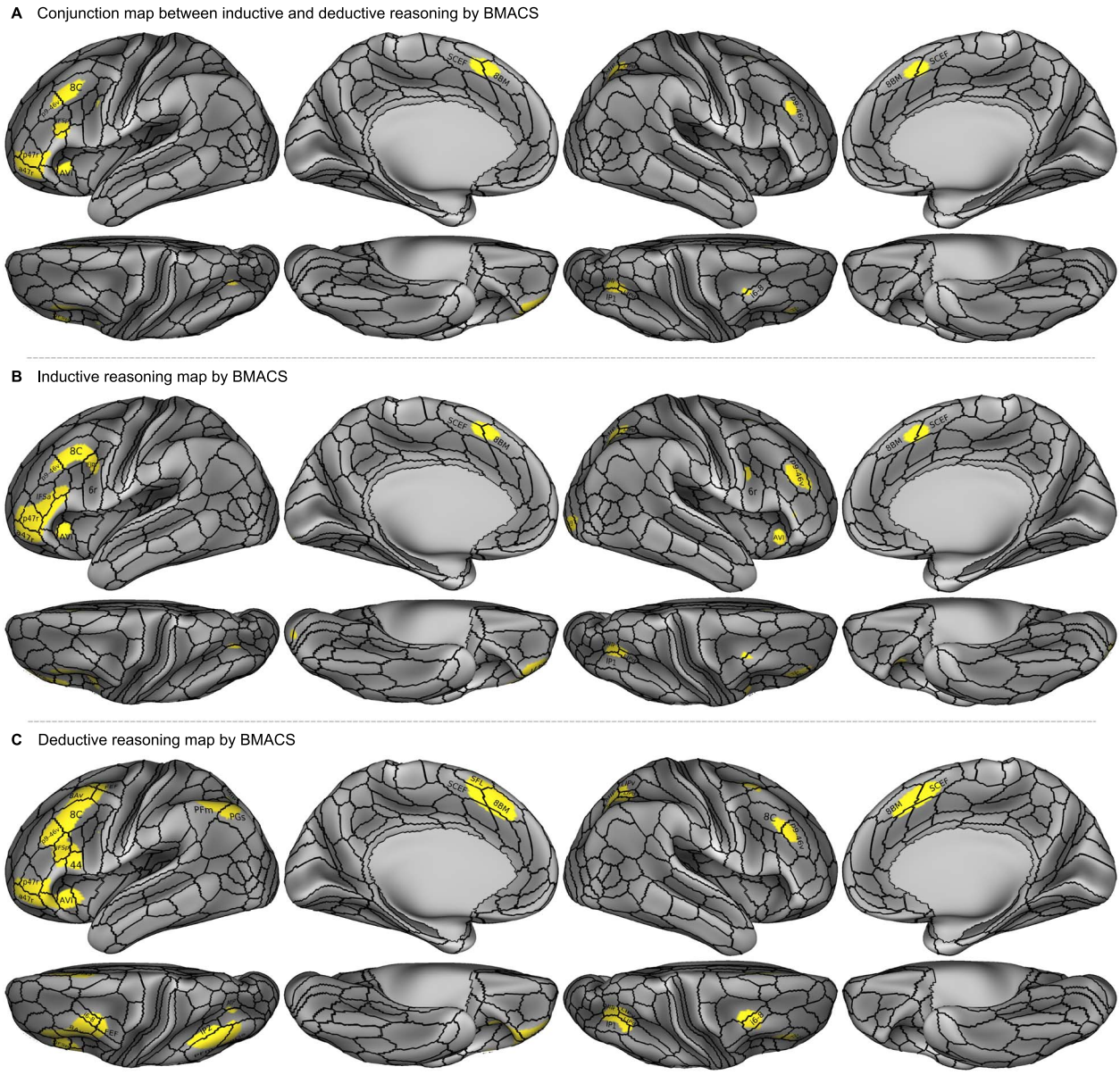

Figure 2. Reasoning-specific maps above 95% exceedance probability. The maps represent brain areas that are highly related to neural process of reasoning, which correspond to regions with above 95% exceedance probability. (*A*) The conjunction map of both inductive and deductive reasoning depicts the regions that were observed in both reasoning-specific maps. (*B*) The map illustrates cortical surface areas related to inductive reasoning. (*C*) The map highlights cortical surface areas related to deductive reasoning. Borders and names of parcels were indicated with 180 parcels per hemisphere, following the multimodal parcellation of the Human Connectome Project (Glasser et al. 2016a). In the Results section, we described regions following the anatomical labeling by Glasser et al. (2016a), where they grouped the 180 parcels into 22 broader regions for readers' readability.

including the dorsolateral prefrontal cortex (8Av, SFL, and i6–8), inferior frontal cortex (44), inferior/superior parietal cortex (PFm, PGs, IP2, and MIP), and premotor cortex (FEF). On the right hemisphere, we found activations in the dorsolateral prefrontal cortex (8C).

Reasoning-Specific Maps Revealed by BMACS in Comparison with MKDA

We compared activation patterns of reasoning obtained from BMACS with those obtained from MKDA. The activation patterns revealed by MKDA show much broader regions compared to BMACS (Fig. 3), which may be linked to reduced specificity of MKDA. We additionally performed MKDA with smaller kernel sizes (namely 6 and 8 mm) to inspect the possibility that kernel size may have affected the result. However, no significant differences were found between the original kernel size (10 mm) and the new sizes (8 mm and 6 mm), resulting in the same conclusion that MKDA shows much broader activation patterns than BMACS.

Better Classification Accuracies in BMACS than in MKDA

Based on a previous study (Kang et al. 2014), we built a classifier to determine whether our posterior predictive maps were

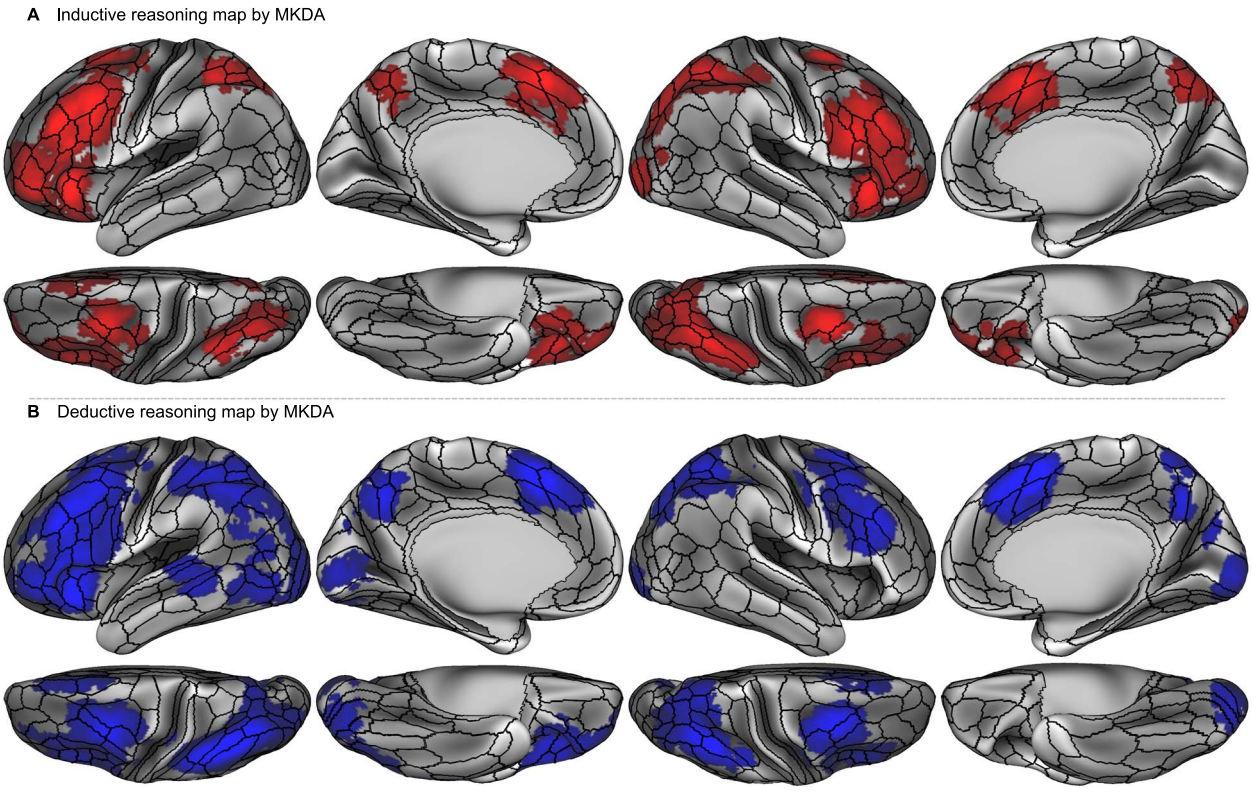

Figure 3. Reasoning-specific maps from MKDA. Colored areas represent the results specific to inductive reasoning (*A*), and deductive reasoning (*B*), being estimated from MKDA that were significant at $P < 0.05$. The results were mapped onto the fs_LR surface for visualization (Van Essen et al. 2012).

able to robustly predict the type of reasoning in comparison with MKDA specifically using a NBC that is widely used for a conventional reverse inference (Yarkoni et al. 2011). By doing this, we aimed to discover which method performed better in terms of classification accuracy, that is, which method captured the spatial patterns associated with inductive and deductive reasoning better.

As a result, BMACS outperformed MKDA. BMACS correctly classified 89.74% of inductive reasoning studies and 74.36% of deductive reasoning studies, with an overall accuracy of 82.05% (Table 1). On the other hand, NBC combined with MKDA correctly classified 76.92% of inductive reasoning studies and 43.59% of deductive reasoning studies, resulting in an overall accuracy of 59.51% (Table 1). This result suggests that BMACS identified the selective activation patterns relevant to each reasoning process better than MKDA.

Validation of BMACS via Successful Reproduction of Results from a Previous Study

To prove that BMACS produces consistent results with other Bayesian methods, we attempted to reproduce 3 core results of a previous Bayesian meta-analysis study (Samartsidis et al. 2019). Consequently, we obtained comparable results to the original study in all the 3 aspects by using BMACS. Firstly, we found that the probability of observing at least one peak coordinate in ROIs for verbal and nonverbal working memory was similar between the original study and BMACS (Table 2). Secondly, we showed that the sample size had no significant effect (Fig. 4A, μ: 0.01, 95% highest density interval [HDI]: [−0.08, 0.09]), likewise in the original study where the HDI included zero. Age was negatively correlated with participants' performance in working memory tasks (Fig. 4B, μ: −0.15, 95% HDI: [−0.24, −0.06]), with the HDI containing the posterior mean of age effect (μ: −0.22) from the original study. Lastly, the distribution of random effects across studies was similar to the original study (Fig. 4C). These results confirm that the performance of BMACS is accurate enough to be compatible with previous time-consuming and complex methods.

Validation of BMACS Via Successful Parameter Recovery

We conducted model validation to verify whether BMACS performs as accurately as expected. We simulated a new dataset from the mean hyperparameters of fitted BMACS that were estimated from the reasoning dataset used in the present study. The hyperparameters here are intercepts for reasoning maps, variance and range parameters for spatial random effects, and a variance parameter for study-specific random effects. We then fitted BMACS to the newly simulated dataset and compared estimated parameters with the true parameters that had been used for the simulation. In our results, most of the true parameters were positioned within the 95% highest density intervals of the estimated parameters except for a slight underestimation of a variance parameter (variance.sf.dR; Fig. 5), showing a successful recovery of the true parameters.

Discussion

In the present study, we proposed a novel Bayesian model-based neuroimaging meta-analysis method of the cortical surface,

Table 1 Comparison of the classification accuracy between BMACS and NBC in combination with MKDA

True label	BMACS		MKDA + NBC	
	Predicted label		Predicted label	
	Inductive	Deductive	Inductive	Deductive
Inductive	89.74	10.26	76.92	23.08
Deductive	25.64	74.36	56.41	43.59
Overall accuracy	82.05		59.51	

Note: The confusion matrix described classification results as the proportion of classified category. The rows represent true reasoning types and columns represent classified reasoning types. For example, BMACS correctly classified 89.74% of inductive reasoning point patterns as inductive reasoning, whereas NBC with MKDA correctly classified 74.36% of inductive reasoning point patterns. Overall, the classification accuracy of BMACS was higher (82.05%) than the combination of MKDA and NBC (59.51%).

Table 2 Reproduction of expected number of activated foci in several ROIs from previous meta-analysis result

ROIs	Original study (Samartsidis et al. 2019)		BMACS	
	Verbal	Nonverbal	Verbal	Nonverbal
Frontal orbital cortex	37.26	36.48	30.70	30.50
Insular cortex	32.79	33.86	28.90	33.60
Precentral gyrus	64.10	72.09	76.10	86.50
Inferior frontal gyrus	43.66	35.69	51.20	43.90
Angular gyrus	24.30	18.91	16.20	15.60
Superior parietal lobule	38.81	33.24	44.50	40.00
Paracingulate gyrus	42.91	49.14	39.60	55.70

Note: We compared probabilities of observing at least one peak coordinate between the original study (Samartsidis et al. 2019) and BMACS. For example, Samartsidis et al. reported that there is a probability of 37.26% that we would observe at least one focus in the frontal orbital cortex during verbal working memory task, while the probability becomes a bit less in nonverbal working memory task of 36.48%. The conclusion that there is a higher probability of observing a focus in frontal orbital cortex during verbal task than nonverbal task remains the same in the result of BMACS (30.70% for verbal task and 30.50% nonverbal task). In all ROIs, the propensity of the original study was well preserved in BMACS whether verbal or nonverbal working memory has higher probability or not.

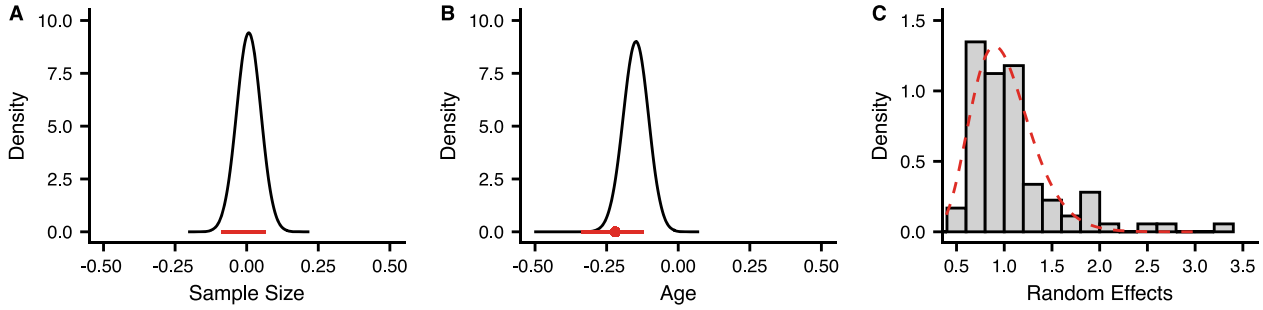

Figure 4. Reproducing the effects from a working memory dataset. The effects of covariates and distribution of random effects were reproduced using BMACS. (*A*) Sample size had no significant effect (μ: 0.01, 95% HDI: [−0.08, 0.09]) on working memory tasks. (*B*) Age was negatively correlated (μ: −0.15, 95% HDI: [−0.24, −0.06]) with performance on working memory tasks. (*C*) The distribution of random effects matched the distribution in the original study (Samartsidis et al. 2019). The red lines in (*A*) and (*B*) illustrate 95% HDIs reported in the original study. The red dot in (*B*) displays the posterior mean. The red dashed line in (*C*) represents the prior Gamma distribution used in the original study.

called BMACS. Using BMACS, we clearly demonstrated inductive- and deductive-specific brain maps, and more importantly, commonly activated regions in both reasoning processes. BMACS, as a model-based approach, has several advantages over conventional meta-analysis methods, such as MKDA or ALE (i.e., kernel-based methods), and overcomes some limitations of previous Bayesian meta-analysis methods.

Understanding of Reasoning along with the Multiple-Demand System

The long-standing and unsolved question among cognitive neuroscientists is how inductive and deductive reasoning are represented at the level of brain networks. With the help of our newly developed Bayesian model-based neuroimaging meta-analysis method of the cortical surface, we show an interesting map of common activations during inductive and deductive reasoning (Fig. 2A), which deserves further discussion. We observed a pattern of activity extending over a specific set of regions, particularly in the dorsolateral prefrontal cortex (8C and p9-46v), orbital and polar frontal cortex (a47r), insular and frontal opercular cortex (AVI), paracentral lobular and mid cingulate cortex (SCEF), and anterior cingulate and medial prefrontal cortex (8BM) in the left hemisphere. This set of regions is known as the multiple-demand (MD) system (Duncan et al. 2000; Duncan 2010), and our maps in Fig. 2A specifically are located in the "core MD" system that were most strongly activated and functionally interconnected in the original study (Assem et al. 2020, 2021;

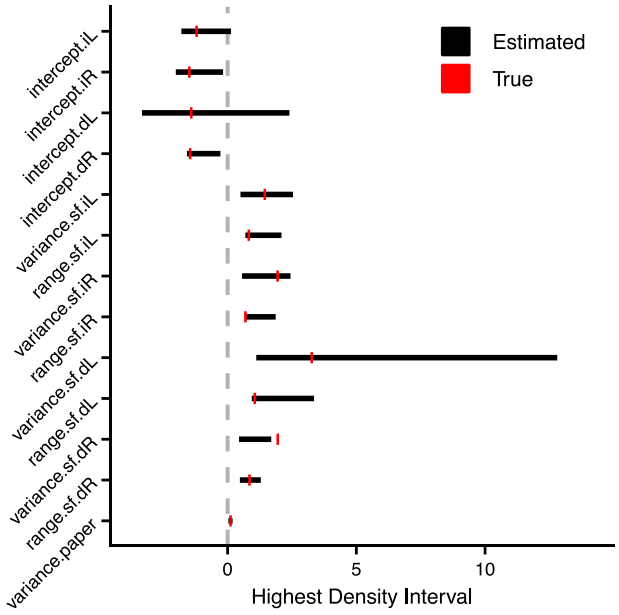

Figure 5. Successful recovery of true parameters. To test whether BMACS could accurately estimate the model parameters, we generated a new dataset from arbitrarily set parameters (i.e., true parameters) and attempted to recover these parameters using BMACS. Most of the parameters were recovered, showing that the true parameters (red lines) were located within the estimated 95% highest density intervals (black lines), except a slight underestimation of a variance parameter (variance.sf.dR). iL, inductive Left; iR, inductive Right; dL, deductive Left; dR, deductive Right; variance.sf/range.sf, variance and range parameters that describe the characteristics of spatial fields with regard to the Matérn covariance structure (Lindgren and Rue 2015).

see Supplementary Fig. S2). The regions in the MD system have been observed repeatedly in numerous functional neuroimaging studies with respect to selective attention, working memory, task switching, response inhibition, conflict monitoring, cognitive control, novel problem-solving, and semantic word processing (Duncan 2010). The MD system has been known to be involved in different kinds of cognitive challenges such as selection of task-relevant stimuli of a current cognitive operation, swift reorganization with changing context, and separation of successive stages of task steps, which are intrinsic to the underlying mechanism for humans' flexible thoughts and problem-solving (Duncan 2010; Woolgar et al. 2018). In fact, this line of processes is closely intertwined with critical components that exert on reasoning (Krawczyk 2018). For example, reasoning deals with multiple inputs such as various premises, conditions, or possibilities, which are transformed into one output, that is, a physical action or a new thought. To do this, selecting task-relevant stimuli, which is one of the functions of the MD system, is obviously involved. However, owing to humans' limited mental resources in perception, attention, and memory, reasoning takes place in multiple steps to draw the most appropriate decision, which pertains to the separation of successive stages of task steps in the MD system. Moreover, reasoning requires the integration of previous knowledge with new information to draw a novel conclusion, and this process is linked to the function of problem-solving in the MD system. Putting all these arguments together, reasoning, which is substantiated by the regional similarity between the core MD system and the conjunction map from the 2 types of reasoning (Fig. 2A), may be construed as a high-level cognitive capability that is unique to humans (Gray and Thompson 2004; Woolgar et al. 2018).

Findings in Inductive- and Deductive-Specific Reasoning

Using BMACS, we showed several brain regions associated with each reasoning process as well. Most of our findings accord with the brain regions that were known to be employed by 1 of the 2 reasoning processes in previous studies. We observed activations in the left inferior frontal cortex and dorsolateral prefrontal cortex, which resemble the activation patterns specific to inductive reasoning in a previous meta-analysis (Wertheim and Ragni 2018). We found a large cluster in the left inferior frontal cortex that has been known to be related to the integration of multiple relations, which is a pivotal process for higher order relational processing during inductive reasoning tasks (Christoff et al. 2001; Cho et al. 2010). Additionally, the right superior parietal cortex was known to maintain spatial information during a relational matching task when participants matched 2 given stimuli in terms of visuospatial concepts (e.g., direction, location, or form) (Wendelken et al. 2012) or applied acquired rules after they learned the unknown relationship within a series of numbers in a reasoning process (Jia and Liang 2015). Furthermore, the right lateralized network that we observed in the present study, including the dorsolateral prefrontal cortex and superior parietal cortex, was more activated when participants drew analogies with complex rules than with simple rules (Hampshire et al. 2011). This network seems to take part in the process of induction, specifically when the cognitive loads increase with respect to reasoning. One thing to note here is that the observed neural activity in the visual cortex may be derived from the effect of study designs since 76 studies out of 78 studies used visual stimuli for reasoning tasks. Collectively, using BMACS, we successfully demonstrated the brain regions known to be actively involved during inductive reasoning.

The deduction-specific regions in our study, such as the left premotor cortex and orbital and polar frontal cortex, have been reported to be activated across multiple deductive reasoning studies in a previous meta-analysis (Prado et al. 2011). Further, the left orbital and polar frontal cortex was exclusively engaged in logical inference compared to linguistic tasks (Monti et al. 2007, 2009), assuring the critical role of these regions in the process of deduction. Activation of the bilateral superior/inferior parietal cortex was also reported in previous deductive reasoning studies, reflecting the process of integrating consecutive arguments during transitive inference (Monti et al. 2007; Brzezicka et al. 2011) or the manipulation of the context-relevant meaning of propositions with respect to combining logical connectives (Baggio et al. 2016). Also, the right prefrontal regions, such as the anterior cingulate and medial prefrontal cortex, and dorsolateral prefrontal cortex, were known to play an important role in inhibiting perceptual bias that helps people to come to a valid conclusion in deductive arguments (Goel and Dolan 2003; Monti et al. 2007; Goel et al. 2009). In summary, our deduction-specific activation map demonstrated brain regions that are crucial for processing deductive arguments.

One caveat to our findings of the reasoning-related set of regions is that we could not include subcortical areas for the BMACS analysis. Previous meta-analyses reported contradicting results regarding the engagement of subcortical areas in reasoning processes. For example, Prado and colleagues (Prado et al.

2011) observed activation of the left basal ganglia across different arguments (i.e., relational, categorical, and propositional arguments) of deductive reasoning. Conversely, Wertheim and Ragni (2018) reported that the engagement of bilateral basal ganglia was specific only to inductive reasoning. Because the estimation of activation patterns of BMACS is confined to the cortical surface, future studies should be conducted that include subcortical regions as target areas for analysis.

We would also like to caution the readers about conceptual interpretation of our results. The current meta-analysis included several different types of contrasts (e.g., contrasts comparing task conditions to baseline conditions or contrasts comparing different task conditions themselves) to maximize the size of dataset and to investigate all the relevant neural processes for reasoning. However, a previous study has shown that despite the same experimental task, different neural patterns can be observed depending on various baseline conditions (Newman et al. 2001). Accordingly, the acquired neural patterns of reasoning in the present study need to be carefully understood within the scope of contrasts we have included. To this end, readers may find the detailed description of included studies and contrasts, which is available from http://doi.org/10.5281/zenodo.4638499.

Advantages of BMACS over Other Methods

BMACS offers 6 advantages over other meta-analytic methods. Firstly, BMACS enables us to directly model the spatial dependence of the data, that is, spatially correlated neural activity between brain areas. In the case of conventional meta-analyses, the inference of consistently activated brain regions is based on null hypothesis significance testing. In other words, the conventional meta-analyses take a mass univariate approach, only searching for voxels that have a greater than random chance to be activated, and as such do not consider spatial dependence of neuroimaging data (Samartsidis et al. 2017). Conversely, with the help of BMACS, we modeled the observed spatial points (i.e., activation foci on the brain) as being generated from latent spatial fields and inferred the spatial patterns for each reasoning process. In our study, we first hypothesized that there would be a spatial map for inductive reasoning studies and another spatial map for deductive reasoning studies. Specifically, we directly modeled studies for each reasoning process to share a common latent spatial field with varying activation strengths in separate studies. Thus, we were able to estimate the general activation patterns for the 2 reasoning processes.

Secondly, it is possible to directly obtain the uncertainty of the parameters, that is, the dispersion of the estimated posterior distributions of model parameters in a Bayesian paradigm (i.e., $\lambda \geq 1$) at any given location on the cortical surface, then define which brain areas are most likely to be observable during a reasoning process. Consequently, we found activation patterns with high confidence by assessing the reliability of the activation strengths across the cortical surfaces and bypassed the problem of multiple comparisons that is unavoidable in most of the conventional meta-analysis methods using a non-Bayesian approach (Bolin and Lindgren 2015).

The third advantage of using BMACS is that the obtained activation maps are highly specific to the core process of a particular cognitive state. As we mentioned earlier, the activation maps for the 2 reasoning processes from BMACS (Fig. 2) show more distinguishable activations than the maps from MKDA (Fig. 3). This third advantage is a natural consequence derived from the first 2 advantages. By incorporating the spatial dependence and uncertainty of the estimated spatial patterns, BMACS seemed to suppress false-positive results. In other words, BMACS demonstrated more selective patterns of activations and higher classification accuracy compared to MKDA, whereupon the brain regions selectively engaged in the specific reasoning process were clearly observed.

The fourth advantage of BMACS is that it is designed to be easily customizable and extensible. To the best of our knowledge, there have only been a few previous studies in which researchers developed new methods adopting Bayesian spatial models for coordinate-based meta-analysis (Kang et al. 2011, 2014; Yue et al. 2012; Montagna et al. 2018; Samartsidis et al. 2019). However, their methods require fine tuning of the algorithm, which makes it difficult to design new model structures (e.g., adding new covariates or modifying how common spatial maps are grouped) because newly implemented models are required to be retuned every time they are introduced. In addition to retuning, the internal structure of the code should be revised to incorporate new model structures, which adds an additional difficulty in testing various hypotheses. In contrast, BMACS is powered by a general Bayesian inference tool, namely INLA (Rue et al. 2009), such that practitioners need not be concerned about additional efforts for fine-tuning the underlying algorithm and can simply focus on establishing model structures or hypotheses. As a result, BMACS has the advantage of being easily extensible into a number of different models.

The fifth advantage of BMACS is a shortened computing time by the significant reduction of computation, which is engendered by adopting a Bayesian posterior approximation tool such as INLA as an alternative to MCMC. The computational bottleneck in previous Bayesian methods was caused by estimating a full covariance function that depicts spatial dependence of the data. Even though some MCMC methods attempted to accelerate the estimation of covariance function by the block Toeplitz matrix (Samartsidis et al. 2019), they still required considerable computing time. For example, Bayesian meta-analysis methods that used MCMC took more than 20 h of computing time (Kang et al. 2014) or even 30 h on a graphics processing unit (Samartsidis et al. 2019). On the contrary, by using INLA, BMACS efficiently approximates the spatial field with a sparse Gaussian Markov random field instead of a full covariance function such that it reduces a significant amount of computation (Lindgren et al. 2011; Simpson et al. 2012; Rue et al. 2017). Correspondingly, fitting BMACS to our reasoning dataset or the working memory dataset (Rottschy et al. 2012) took only 1 or 2 h in approximation, respectively.

The final advantage of BMACS is the proper consideration of the spatial dependence between brain areas. In Bayesian meta-analysis methods, the squared exponential function has been commonly used as a covariance function to consider the spatial correlations, and Euclidean distance has been used as a distance measure between brain areas (i.e., voxels) for the covariance function (Montagna et al. 2018; Samartsidis et al. 2019). However, the actual distance between brain areas is more appropriately represented by the distance defined along the cortical surface, since the human brain exhibits a folded cortical surface structure (Mejia et al. 2020). By adopting cortical surface-based analysis, BMACS represents the spatial dependence of brain data more realistically (Mejia et al. 2020). Additionally, we used the Matérn covariance structure, which is a more flexible function than the commonly used squared exponential covariance function

(Lindgren et al. 2011; Simpson et al. 2012; Samartsidis et al. 2019), as a function of spatial dependence such that we were able to apprehend the true spatial pattern more accurately.

Overall, BMACS, while preserving the advantage of a model-based approach, eliminated most of the difficulties found in previous model-based methods, as it circumvents a huge amount of computing time and extends easily to various model structures. In addition, to the best of our knowledge, BMACS is the first Bayesian meta-analysis method that uses cortical surface-based analysis.

Limitations of BMACS

Nonetheless, a few limitations lie in the current method, BMACS, which need to be addressed in future studies. Firstly, we were unable to apply BMACS to the studies that performed group-level analysis of the cortical surface. The major problem of coordinate-based meta-analyses is the use of peak coordinates obtained from volume-based analyses. The methods are known to lack precise localization, and thus, it has been recommended to use surface-based methods instead (Coalson et al. 2018). However, sharing cortical surface data has not been a common practice in the neuroimaging community, although the Human Connectome Project has strived for putting surface-based methods into practice and sharing large-scale cortical surface data (Glasser, Smith, et al. 2016b). Therefore, it was difficult for us to obtain the necessary cortical surface data with regard to reasoning. Researchers share their results using open-source databases such as NeuroVault (https://neurovault.org) or OpenNeuro (https://openneuro.org) nowadays, but most of these data are released in the format of volumetric space. Thus, under the current circumstances, we did our best to reach the most appropriate compromise by developing BMACS. Fortunately, the brain analysis library of spatial maps and atlases (BALSA; https://balsa.wustl.edu) recently started to offer a repository to upload surface-based dataset, and we believe this database will promote sharing cortical surface-based data (Van Essen et al. 2017).

The second limitation is potential inaccuracies during the process of mapping peak coordinates from the volumetric space to the cortical surface. We used the state-of-the-art mapping method described in Wu et al. (2018) to minimize distortion during the coordinate system conversion. However, as stated in the original study (Wu et al. 2018), the ideal way of representing brain data on the cortical surface would be through directly registering the raw data to the cortical surface coordinate system, if possible. Unfortunately, to the best of our knowledge, this suggestion is currently very challenging due to the aforementioned problem (the lack of open-source cortical surface data in reasoning). We hope for researchers to pay more attention to cortical surface-based analysis and to share cortical surface data in the neuroimaging community (Tucholka et al. 2012; Mejia et al. 2020).

Conclusion

To summarize, using BMACS we revealed the core regions associated with both inductive and deductive reasoning types, which conform to the core MD system. Therefore, we suggest that the reasoning process occurs in a dynamic way, being closely interwoven with numerous cognitive processes and being intrinsic to human high-level cognition. We posit BMACS as a tool that provides a fast, reliable, and accessible coordinate-based meta-analysis that robustly estimates the activation patterns of the cortical surface's targeted cognitive processes. However, the outcomes reported in the current study should be interpreted carefully because of the limitations that BMACS embodies. Furthermore, we call for the future meta-analysis studies that involve individual cortical surface-based studies. We hope that BMACS will advance toward the use of cortical surface-based meta-analysis and that it will be of great help in unveiling neural mechanisms of diverse cognitive processes.

Supplementary Material

Supplementary material can be found at *Cerebral Cortex* online.

Funding

This work was supported by the National Research Foundation of Korea (2020R1A2C2099568, 2019M3C7A1031995, 2017M3A9G8084463).

Notes

We thank Shameem Wagner for proofreading in English. We also thank Finn Lindgren for constructive discussion and consultation on INLA. *Conflict of Interest*: The authors declare no competing interests.

Authors' Contributions (CRediT Taxonomy)

Conceptualization: M.S. and H.-A.J; Methodology: M.S.; Software: M.S.; Formal Analysis: M.S.; Writing—Original Draft: M.S. and H.-A.J.; Writing—Review & Editing: M.S. and H.-A.J.; Visualization: M.S.; Supervision: H.-A.J.; Project Administration: H.-A.J.; Funding Acquisition: H.-A.J.

References

Assem M, Glasser MF, Van Essen DC, Duncan J. 2020. A domain-general cognitive core defined in multimodally parcellated human cortex. *Cereb Cortex*. 30:4361–4380.

Assem M, Shashidhara S, Glasser MF, Duncan J. 2021. Precise topology of adjacent domain-general and sensory-biased regions in the human brain. *bioRxiv*. https://doi.org/10.1101/2021.02.21.431622

Baggio G, Cherubini P, Pischedda D, Blumenthal A, Haynes JD, Reverberi C. 2016. Multiple neural representations of elementary logical connectives. *NeuroImage*. 135:300–310.

Bolin D, Lindgren F. 2015. Excursion and contour uncertainty regions for latent Gaussian models. *J Roy Stat Soc Ser B (Stat Method)*. 77:85–106.

Botvinik-Nezer R, Holzmeister F, Camerer CF, Dreber A, Huber J, Johannesson M, Kirchler M, Iwanir R, Mumford JA, Adcock RA, et al. 2020. Variability in the analysis of a single neuroimaging dataset by many teams. *Nature*. 582:84–88.

Bowman FD. 2005. Spatio-temporal modeling of localized brain activity. *Biostatistics*. 6:558–575.

Brett M, Christoff K, Cusack R, Lancaster J. 2001. Using the Talairach atlas with the MNI template. *NeuroImage*. 13:85.

Brzezicka A, Sedek G, Marchewka A, Gola M, Jednorog K, Krolicki L, Wrobel A. 2011. A role for the right prefrontal and bilateral parietal cortex in four-term transitive reasoning: an fMRI study with abstract linear syllogism tasks. *Acta Neurobiol Exp (Wars)*. 71:479–495.

Button KS, Ioannidis JPA, Mokrysz C, Nosek BA, Flint J, Robinson ESJ, Munafò MR. 2013. Power failure: why small sample size undermines the reliability of neuroscience. *Nat Rev Neurosci*. 14:365.

Cho S, Moody TD, Fernandino L, Mumford JA, Poldrack RA, Cannon TD, Knowlton BJ, Holyoak KJ. 2010. Common and dissociable prefrontal loci associated with component mechanisms of analogical reasoning. *Cereb Cortex*. 20: 524–533.

Christoff K, Prabhakaran V, Dorfman J, Zhao Z, Kroger JK, Holyoak KJ, Gabrieli JD. 2001. Rostrolateral prefrontal cortex involvement in relational integration during reasoning. *NeuroImage*. 14:1136–1149.

Coalson TS, Van Essen DC, Glasser MF. 2018. The impact of traditional neuroimaging methods on the spatial localization of cortical areas. *Proc Natl Acad Sci*. 115:E6356–E6365.

Dale AM, Fischl B, Sereno MI. 1999. Cortical surface-based analysis: I. segmentation and surface reconstruction. *NeuroImage*. 9:179–194.

Diggle PJ, Moraga P, Rowlingson B, Taylor BM. 2013. Spatial and spatio-temporal log-Gaussian cox processes: extending the geostatistical paradigm. *Stat Sci*. 28:542–563.

Duncan J. 2010. The multiple-demand (MD) system of the primate brain: mental programs for intelligent behaviour. *Trends Cogn Sci*. 14:172–179.

Duncan J, Seitz RJ, Kolodny J, Bor D, Herzog H, Ahmed A, Newell FN, Emslie H. 2000. A neural basis for general intelligence. *Science*. 289:457–460.

Eickhoff SB, Laird AR, Grefkes C, Wang LE, Zilles K, Fox PT. 2009. Coordinate-based activation likelihood estimation meta-analysis of neuroimaging data: a random-effects approach based on empirical estimates of spatial uncertainty. *Hum Brain Mapp*. 30:2907–2926.

Fischl B, Sereno MI, Tootell RBH, Dale AM. 1999. High-resolution intersubject averaging and a coordinate system for the cortical surface. *Hum Brain Mapp*. 8:272–284.

Gamerman D, Lopes HF. 2006. *Markov Chain Monte Carlo: stochastic simulation for Bayesian inference*. Second ed. Boca Raton: Chapman & Hall/CRC.

Gelfand AE. 1996. Model determination using sampling-based methods. In: Gilks WR, Richardson S, Spiegelhalter DJ, editors. *Markov chain Monte Carlo in practice*. 1st ed. Boca Raton: Chapman and Hall/CRC, pp. 145–161.

Gelfand AE, Dey DK, Chang H. 1992. Model determination using predictive distributions with implementation via sampling-based methods (with discussion). In: Bernardo JM, Berger JO, Dawid AP, Smith AFM, editors. *Bayesian statistics* 4. 1st ed. Oxford: Clarendon Press, pp. 147–167.

Glasser MF, Coalson TS, Robinson EC, Hacker CD, Harwell J, Yacoub E, Ugurbil K, Andersson J, Beckmann CF, Jenkinson M, et al. 2016a. A multi-modal parcellation of human cerebral cortex. *Nature*. 536:171–178.

Glasser MF, Smith SM, Marcus DS, Andersson JLR, Auerbach EJ, Behrens TEJ, Coalson TS, Harms MP, Jenkinson M, Moeller S, et al. 2016b. The Human Connectome Project's neuroimaging approach. *Nat Neurosci*. 19:1175–1187.

Goel V. 2005. Cognitive neuroscience of deductive reasoning. In: Holyoak KJ, Morrison RG, editors. *The Cambridge handbook of thinking and reasoning*. 1st ed. New York: Cambridge University Press, pp. 475–492.

Goel V. 2007. Anatomy of deductive reasoning. *Trends Cogn Sci*. 11:435–441.

Goel V, Dolan RJ. 2003. Reciprocal neural response within lateral and ventral medial prefrontal cortex during hot and cold reasoning. *NeuroImage*. 20:2314–2321.

Goel V, Stollstorff M, Nakic M, Knutson K, Grafman J. 2009. A role for right ventrolateral prefrontal cortex in reasoning about indeterminate relations. *Neuropsychologia*. 47:2790–2797.

Gray JR, Thompson PM. 2004. Neurobiology of intelligence: science and ethics. *Nat Rev Neurosci*. 5:471–482.

Green AE, Kraemer DJ, Fugelsang JA, Gray JR, Dunbar KN. 2010. Connecting long distance: semantic distance in analogical reasoning modulates frontopolar cortex activity. *Cereb Cortex*. 20:70–76.

Hampshire A, Thompson R, Duncan J, Owen AM. 2011. Lateral prefrontal cortex subregions make dissociable contributions during fluid reasoning. *Cereb Cortex*. 21:1–10.

Hayes BK, Heit E, Rotello CM. 2014. Memory, reasoning, and categorization: parallels and common mechanisms. *Front Psychol*. 5:1–9.

Heit E, Rotello CM. 2010. Relations between inductive reasoning and deductive reasoning. *J Exp Psychol Learn Mem Cogn*. 36:805–812.

Hobeika L, Diard-Detoeuf C, Garcin B, Levy R, Volle E. 2016. General and specialized brain correlates for analogical reasoning: a meta-analysis of functional imaging studies. *Hum Brain Mapp*. 37:1953–1969.

Jia X, Liang P. 2015. The relationship of four brain regions to an information-processing model of numerical inductive reasoning process: an fMRI study. *J Adv Neurosci Res*. 2: 7–22.

Kang J, Johnson TD, Nichols TE, Wager TD. 2011. Meta-analysis of functional neuroimaging data via Bayesian spatial point processes. *J Am Stat Assoc*. 106:124–134.

Kang J, Nichols TE, Wager TD, Johnson TD. 2014. A Bayesian hierarchical spatial point process model for multi-type neuroimaging meta-analysis. *Ann Appl Stat*. 8:1800–1824.

Klauer KJ, Phye GD. 2008. Inductive reasoning: a training approach. *Rev Educ Res*. 78:85–123.

Krawczyk DC. 2018. Introduction to Reasoning. In: Krawczyk DC, editor. *Reasoning: the neuroscience of how we think*. 1st ed. London: Academic Press, pp. 1–11.

Lancaster JL, Tordesillas-Gutiérrez D, Martinez M, Salinas F, Evans A, Zilles K, Mazziotta JC, Fox PT. 2007. Bias between MNI and Talairach coordinates analyzed using the ICBM-152 brain template. *Hum Brain Mapp*. 28:1194–1205.

Lindgren F, Rue H. 2015. Bayesian spatial modelling with R-INLA. *J Stat Softw*. 63:1–25.

Lindgren F, Rue H, Lindström J. 2011. An explicit link between Gaussian fields and Gaussian Markov random fields: the stochastic partial differential equation approach. *J Roy Stat Soc Ser B (Stat Method)*. 73:423–498.

Marcus DS, Harwell J, Olsen T, Hodge M, Glasser MF, Prior F, Jenkinson M, Laumann T, Curtiss SW, Van Essen DC. 2011. Informatics and data mining tools and strategies for the Human Connectome Project. *Front Neuroinform*. 5:4.

McAbee ST, Landis RS, Burke MI. 2017. Inductive reasoning: the promise of big data. *Hum Resour Manag Rev*. 27:277–290.

Mejia AF, Yue Y, Bolin D, Lindgren F, Lindquist MA. 2020. A Bayesian general linear modeling approach to cortical surface fMRI data analysis. *J Am Stat Assoc*. 115:501–520.

Moher D, Liberati A, Tetzlaff J, Altman DG, The PG. 2009. Preferred reporting items for systematic reviews and meta-analyses: the PRISMA statement. *PLoS Med*. 6:e1000097.

Møller J, Syversveen AR, Waagepetersen RP. 1998. Log Gaussian Cox processes. *Scand J Stat*. 25:451–482.

Montagna S, Wager T, Barrett LF, Johnson TD, Nichols TE. 2018. Spatial Bayesian latent factor regression modeling of coordinate-based meta-analysis data. *Biometrics*. 74:342–353.

Monti MM, Osherson DN, Martinez MJ, Parsons LM. 2007. Functional neuroanatomy of deductive inference: a language-independent distributed network. *NeuroImage*. 37:1005–1016.

Monti MM, Parsons LM, Osherson DN. 2009. The boundaries of language and thought in deductive inference. *Proc Natl Acad Sci*. 106:12554–12559.

Müller VI, Cieslik EC, Laird AR, Fox PT, Radua J, Mataix-Cols D, Tench CR, Yarkoni T, Nichols TE, Turkeltaub PE, et al. 2018. Ten simple rules for neuroimaging meta-analysis. *Neurosci Biobehav Rev*. 84:151–161.

Newman SD, Twieg DB, Carpenter PA. 2001. Baseline conditions and subtractive logic in neuroimaging. *Hum Brain Mapp*. 14:228–235.

Penn DC, Holyoak KJ, Povinelli DJ. 2008. Darwin's mistake: explaining the discontinuity between human and nonhuman minds. *Behav Brain Sci*. 31:109–130.

Penny WD, Trujillo-Barreto NJ, Friston KJ. 2005. Bayesian fMRI time series analysis with spatial priors. *NeuroImage*. 24:350–362.

Poldrack R. 2006. Can cognitive processes be inferred from neuroimaging data? *Trends Cogn Sci*. 10:59–63.

Prado J, Chadha A, Booth JR. 2011. The brain network for deductive reasoning: a quantitative meta-analysis of 28 neuroimaging studies. *J Cogn Neurosci*. 23:3483–3497.

Rodriguez-Moreno D, Hirsch J. 2009. The dynamics of deductive reasoning: an fMRI investigation. *Neuropsychologia*. 47:949–961.

Rottschy C, Langner R, Dogan I, Reetz K, Laird AR, Schulz JB, Fox PT, Eickhoff SB. 2012. Modelling neural correlates of working memory: a coordinate-based meta-analysis. *NeuroImage*. 60:830–846.

Rue H, Martino S, Chopin N. 2009. Approximate Bayesian inference for latent Gaussian models by using integrated nested Laplace approximations. *J Roy Stat Soc Ser B (Stat Method)*. 71:319–392.

Rue H, Riebler A, Sørbye SH, Illian JB, Simpson DP, Lindgren FK. 2017. Bayesian computing with INLA: a review. *Annu Rev Stat Appl*. 4:395–421.

Samartsidis P, Eickhoff CR, Eickhoff SB, Wager TD, Barrett LF, Atzil S, Johnson TD, Nichols TE. 2019. Bayesian log-Gaussian Cox process regression: applications to meta-analysis of neuroimaging working memory studies. *J Roy Stat Soc Ser C (Appl Stat)*. 68:217–234.

Samartsidis P, Montagna S, Johnson TD, Nichols TE. 2017. The coordinate-based meta-analysis of neuroimaging data. *Stat Sci*. 32:580–599.

Simpson D, Illian JB, Lindgren F, Sørbye SH, Rue H. 2016. Going off grid: computationally efficient inference for log-Gaussian Cox processes. *Biometrika*. 103:49–70.

Simpson D, Lindgren F, Rue H. 2012. In order to make spatial statistics computationally feasible, we need to forget about the covariance function. *Environmetrics*. 23:65–74.

Tucholka A, Fritsch V, Poline J-B, Thirion B. 2012. An empirical comparison of surface-based and volume-based group studies in neuroimaging. *NeuroImage*. 63: 1443–1453.

Turkeltaub PE, Eden GF, Jones KM, Zeffiro TA. 2002. Meta-analysis of the functional neuroanatomy of single-word reading: method and validation. *NeuroImage*. 16: 765–780.

Van Essen DC, Glasser MF, Dierker DL, Harwell J, Coalson T. 2012. Parcellations and hemispheric asymmetries of human cerebral cortex analyzed on surface-based atlases. *Cereb Cortex*. 22:2241–2262.

Van Essen DC, Smith J, Glasser MF, Elam J, Donahue CJ, Dierker DL, Reid EK, Coalson T, Harwell J. 2017. The Brain Analysis Library of Spatial maps and Atlases (BALSA) database. *NeuroImage*. 144:270–274.

Wager TD, Lindquist M, Kaplan L. 2007. Meta-analysis of functional neuroimaging data: current and future directions. *Soc Cogn Affect Neurosci*. 2:150–158.

Wager TD, Lindquist MA, Nichols TE, Kober H, Van Snellenberg JX. 2009. Evaluating the consistency and specificity of neuroimaging data using meta-analysis. *NeuroImage*. 45:S210–S221.

Wendelken C. 2015. Meta-analysis: how does posterior parietal cortex contribute to reasoning? *Front Hum Neurosci*. 8: 1042.

Wendelken C, Chung D, Bunge SA. 2012. Rostrolateral prefrontal cortex: domain-general or domain-sensitive? *Hum Brain Mapp*. 33:1952–1963.

Wertheim J, Ragni M. 2018. The neural correlates of relational reasoning: a meta-analysis of 47 functional magnetic resonance studies. *J Cogn Neurosci*. 30:1734–1748.

Woolgar A, Duncan J, Manes F, Fedorenko E. 2018. Fluid intelligence is supported by the multiple-demand system not the language system. *Nat Hum Behav*. 2:200–204.

Wu J, Ngo GH, Greve D, Li J, He T, Fischl B, Eickhoff SB, Yeo BTT. 2018. Accurate nonlinear mapping between MNI volumetric and free surfer surface coordinate systems. *Hum Brain Mapp*. 39:3793–3808.

Yarkoni T, Poldrack RA, Nichols TE, Van Essen DC, Wager TD. 2011. Large-scale automated synthesis of human functional neuroimaging data. *Nat Methods*. 8:665–670.

Yue YR, Lindquist MA, Loh JM. 2012. Meta-analysis of functional neuroimaging data using Bayesian nonparametric binary regression. *Ann Appl Stat*. 6:697–718.